FERMILAB-CONF-74-117-E

One-Particle and Two-Particle Distributions and Correlations in 205 GeV/c $\pi^- p$ Inclusive Reactions* †

W.D. Shephard, V.P. Kenney, J.M. Bishop
N.N. Biswas, N.M. Cason, E.D. Fokitis

University of Notre Dame

W.D. Walker, J.S. Loos, L. Fortney, A. Goshaw, W. Robertson

Duke University

B.J. Deery, D.M. Harrison, G. Hartner, G. Levman,
J.D. Prentice, P.M. Patel, V.A. Sreedhar, S. Vallet, T.S. Yoon

Institute of Particle Physics of Canada

Abstract. New data are presented for 205 GeV/c $\pi^- p$ inclusive reactions from a preliminary sample obtained with the 30-inch bubble chamber-wide gap spark chamber hybrid spectrometer at NAL. Single-particle distributions are studied in terms of factorization and approach to scaling in the target fragmentation region. In the central region of c.m.s. rapidity, plateau development is evident. Two-particle rapidity distributions and correlations are presented for all charged particles and for pions of the same and of opposite charge. Plateau development is also seen in the two-particle distributions. There is evidence of significant short range correlations, consistent with a correlation length $\lambda \approx 1.5$, for the inclusive reactions. Correlations for semi-inclusive reactions as a function of charged-particle multiplicity are also studied and the results are contrasted with the corresponding correlations for the inclusive reactions.

† Presented by V.P. Kenney

I. PROCEDURE

In this report we present new data on the inclusive production of negative and positive pions in 205 GeV/c $\pi^- p$ interactions at NAL. The πp inclusive reactions are of special interest in that they allow the target and projectile systems to be distinguished. In order to realize this advantage, our experiment makes use of the Exp. 2B hybrid spectrometer arrangement of Fig. 1a. Four dual wide-gap optical spark chambers are set up downstream from the NAL 30-in. (76 cm) bubble chamber to permit the measurement of fast, forward secondaries with high precision. A system of proportional wire chambers upstream (from the Exp. 154 consortium) defines the positions and directions of beam particles which interact in the bubble chamber and trigger the wide-gap spark chamber system.

The trigger arrangement is shown in Figure 1a. A trigger is generated if an incoming beam track either (i) produces two or more forward secondary tracks as detected in a set of three 1/16 inch (1.59 mm) dE/dx counters located in the beam-exit gap of the bubble chamber magnet, or (ii) is deflected from a normal beam trajectory in passing between two sets of aligned "finger counters", one upstream and one downstream of the bubble chamber. Since the dE/dx trigger efficiency increases with multiplicity while the beam deflection trigger is most efficient with low-multiplicity events, the two triggers, operated in the OR mode, are complementary.

The wide-gap spark chambers themselves are 8 in. (20.3 cm) deep with an active area of 30 in. (76.2 cm) horizontal x 40 in. (101.6 cm)

vertical. The chambers are arranged approximately 1 meter apart, beginning at a point 4 meters downstream from the center of the bubble chamber. Each of the four dual chamber modules is fired by a ten-stage Marx generator running typically at 22-28 kV per stage with a width of ~60 nsec. Track images are recorded on 35 mm film, each frame containing a direct view, a 90° mirror view, and a 10° mirror view.

We have taken some 120,000 sets of bubble chamber pictures together with spark chamber pictures for all dE/dx and beam-deflection triggers. In addition, we have operated our wide-gap system behind the NAL-Berkeley "bare bubble chamber" Exp. 137 during the tuning of our spark chamber trigger, obtaining a further 40,000 bubble-chamber pictures[1] together with spark-chamber pictures primarily for dE/dx triggers. The data reported here are from this preliminary 40,000-picture run.

The advantage of the hybrid system for fast forward secondaries is illustrated in Fig. 1b in which momentum error $\Delta p/p$ is plotted against particle momentum for a typical sample of track measurements. The combined bubble chamber-wide gap chamber "hook-up" measurements (O symbol) concentrate along the lower boundary of the scatter plot, while the measurements obtained with the bubble-chamber alone (x symbol) generally have much larger $\Delta p/p$ error. In the present preliminary run we replace the bubble-chamber measurement of at least one secondary track with the more accurate combined bubble chamber-spark chamber measurement in ~45% of all bubble chamber events. For our 120,000

picture final run, where an improved beam deflection trigger as well as the dE/dx trigger were operational, this percentage is higher.

II. INCLUSIVE SINGLE PARTICLE DISTRIBUTIONS

The invariant differential cross sections $d\sigma/(d^3p/E)$ for inclusive single-particle production have been studied as a function of longitudinal and transverse momentum variables. In Figs. 2a and 2b are shown distributions of $(2E/\pi\sqrt{s})(d\sigma/dx)$ as a function of the Feynman variable x for secondary π^- and π^+ mesons[2]. In the region $x < +0.2$ ($p_{lab} \lesssim 40$ GeV/c) all reconstructed tracks have been included. Momenta from combined bubble chamber-spark chamber "hook-up" reconstructions are used wherever possible. For $x > +0.2$ we have utilized the improved momentum resolution of the hybrid spectrometer by including only "hook-up" tracks in the sample. Since most of the preliminary run included only spark-chamber triggers from events with two fast forward tracks elastic events are effectively eliminated. Also eliminated in the $x > +0.2$ region are contributions corresponding to tracks from events involving only one fast-forward particle (e.g. most low-multiplicity events in which only the target proton dissociates). Data from our final run will allow a better determination of the cross section for large positive x. To obtain an estimate of the absolute differential cross section for $x > +0.2$, the distributions of "hooked-up" tracks have been weighted by the ratio of "all tracks" to "hooked-up" tracks in this region. Since even some of the "hooked-up" tracks have reconstructed momenta corresponding to $x > 1.0$, we have tried several methods of including these tracks[3] in the distribution.

The "$\mp$" points in Fig. 2 were determined by multiplying values for $x > +0.2$ by an additional constant to account for the tracks with $x > 0$. The superimposed "x" points were calculated by distributing these tracks uniformly in x over the region $0.45 < x < 1.0$ and by assuming that they have c.m. energy corresponding to the mean energy for tracks in a given bin. We plan to try kinematic fitting on these events as a further method of distributing them.

Lower energy data for 18.5 GeV/c (Notre Dame)[4] and 40 GeV/c (Alma-Ata, Bucharest, Budapest, Cracow, Dubna, Hanoi, Serpukhov, Sofia, Tashkent, Tbilisi, Ulan-Bator, Warsaw Collaboration)[5] incident π^- are shown for comparison. The $\pi^- p \to \pi^- + \ldots$ distributions in particular remind those of us who have become accustomed to pp data from the ISR that there is no reason to expect forward-backward symmetry. Leading-particle effects, however, appear less prominent as the incident energy increases.

Distributions of $d\sigma/dp_T^2$ as a function of p_T^2 for secondary π^- and π^+ are shown in Figs. 3a and 3b respectively. Comparison of the two figures indicates that the p_T^2 distributions appear the same regardless of pion charge and are shifted uniformly higher compared with the 18.5 GeV/c distributions shown for comparison. The shift observed in the region $p_T^2 < 1 (\mathrm{GeV/c})^2$ is consistent with the observed increase in the numbers of secondary π^- and π^+ mesons with increasing incident momenta.

The invariant structure function $\pi^{-1} d\sigma/dy$ (the invariant differen-

tial cross section integrated over all transverse momenta) is shown as a function of c.m. rapidity y for secondary π^- and π^+ in Figs. 4a and 4b respectively. The 18.5 GeV/c and 40 GeV/c data are again presented for comparison. Both distributions show the expected growth with increasing $\sqrt{s}$ and both suggest significant plateau development in the central region. The plateau appears most pronounced for the produced π^+, where it extends over three units of rapidity from $-1.5 \leq y \leq 1.5$. There seems to be evidence of an approach to scaling in the central region although the invariant cross section near $y = 0$ may still be increasing in this energy region. When the rapidity distributions for the 18.5 GeV/c and 40 GeV/c data are "boosted" so that they can be compared in the target rest frame there is good agreement in the target fragmentation region with the 205 GeV/c data; when they are "boosted" to the projectile rest frame, the lower-energy points tend to lie above the 205 GeV/c data, especially in the π^- case, consistent with the decrease in leading-particle effects suggested by the x distributions of Fig. 2.

For the target and projectile fragmentation regions, it has been suggested[6] that the single particle inclusive amplitude can be described by the exchange of the Regge singularities occurring in 2-body scattering. Calculations assuming factorization of Regge residues then predict that the distributions in the target (projectile) fragmentation regions should be independent of the type of projectile (target) involved. The y distribution for π^- produced in 205 GeV/c pp reactions[7] (observed with the same experimental arrangement as this experiment) normalized to

the $\pi^- p$ total cross section is shown together with the 205 GeV/c $\pi^- p \rightarrow \pi^- + \ldots$ data in Fig. 5a. The data are in good agreement in the target fragmentation region (in the entire backward hemisphere, in fact) indicating that factorization is good to at least the 10% level of statistics. That the proton fragmentation to π^- is relatively independent of projectile momentum in $\pi^- p$ as well as in pp interactions is again illustrated in Fig. 5b where the 205 GeV/c distribution is again shown together with the 18.5 GeV/c and 40 GeV/c distributions boosted to the target rest frame for direct comparison.

In Figs. 6a and 6b we have added new data to two figures published previously in a Berkeley-Notre Dame study[8] of the approach to scaling at lower energies. The approach to scaling in the central region is shown in Fig. 6a, where the value of the structure function in the interval $-0.02 \leq x \leq 0.02$ is plotted as a function of $s^{-1/4}$ as suggested by Mueller-Regge theory. The equality of the $x = 0$ structure function values for produced π^- and π^+ at 205 GeV/c is striking. There is clear indication that the structure function for the central region has not reached its limiting value in the 205 GeV/c data but continues to increase, perhaps to intersect the continuation of the $\pi^+ p \rightarrow \pi^- + \ldots$ at the "Ferbel point", $C/\pi = 0.25$. The integral of the structure function $G(p_{\parallel}) = \int (E/\sigma_T)(d^2\sigma/dp_{\parallel}\, dp_T^2) dp_T^2$ for $p_{\parallel} < 0$ in the laboratory system is shown as a function of $s^{-1/2}$ in Fig. 6b. The new data point at 205 GeV/c remains consistent with the $a + b\, s^{-1/2}$ approach to scaling in the target rest system suggested by Mueller-Regge theory.

III. TWO-PARTICLE DISTRIBUTIONS AND CORRELATIONS

While single-particle distributions for inclusive reactions are capable of providing useful insights into some characteristics of the reactions (e.g. the approach to scaling), they do not provide complete information and do not appear to allow a clear discrimination among possible mechanisms of particle production. More information can be obtained from the two-particle inclusive reactions via a study of double differential cross sections and of correlation functions. For the basic two-body inclusive reaction $a + b \rightarrow c_1 + c_2 + \ldots$ where c_1 and c_2 may be particles of the same type or of different types the invariant double-differential cross section is $d\sigma/(d^3p_1/E_1)(d^3p_2/E_2)$.

Various types of correlations in the production of two particles may be postulated and the data may be appropriately plotted to see if significant correlations are present. Here we present results on correlations in c.m. rapidity y. After integration over all transverse momenta the invariant double-differential cross section in terms of the rapidities is

$$\pi^{-2} d\sigma/dy_1 dy_2$$

It is customary to define a normalized two-particle distribution function,

$$\rho_2(y_1, y_2) = \sigma_{inel}^{-1} d\sigma/dy_1 dy_2$$

and a normalized single-particle distribution function,

$$\rho_1(y) = \sigma_{inel}^{-1} d\sigma/dy .$$

Common forms for inclusive correlation functions in rapidity are:

$$R(y_1, y_2) = \frac{\rho_2(y_1, y_2)}{\rho_1(y_1)\rho_1(y_2)} - 1 = \frac{\sigma_{inel}(d\sigma/dy_1 dy_2)}{(d\sigma/dy_1)(d\sigma/dy_2)} - 1$$

and

$$C(y_1, y_2) = \rho_2(y_1, y_2) - \rho_1(y_1)\rho_1(y_2)$$
$$= \sigma_{inel}^{-1}(d\sigma/dy_1 dy_2) - \sigma_{inel}^{-2}(d\sigma/dy_1)(d\sigma/dy_2)$$

In both cases a value of zero would be consistent with no correlation. Since $R(y_1, y_2)$ is less dependent on the absolute normalization, it has more commonly been presented. We will follow this convention so that our results may be easily compared with other available data.

An exciting result in two-particle correlation studies has been the observation at ISR[9,10] and at NAL[11] of positive short-range correlations in the central region in pp interactions. For correlations involving two charged particles or charged particles and gammas, the ISR results, displayed as contour plots of constant $R(\eta_1, \eta_2)$ as a function of η_1 and η_2 (where $\eta = \ln \tan(\theta_{c.m.}/2)$ is an approximation to c.m. rapidity y for $p_T^2 >> m^2$), show the contours elongated parallel to $\eta_1 = \eta_2$ in the central region so that $R(\eta_1, \eta_2)$ is primarily a function of $\Delta\eta = |\eta_2 - \eta_1|$. The central value, $R(0, 0)$, is strongly positive with a value of about +0.65. These features of the plots are interpreted as indicating positive short-range correlations between the produced particles. Various other features are observed including increased separation of contours along $\eta_1 = -\eta_2$ and positive values of R in regions where one particle has large positive η and the other has large negative η. These long-range correlations are suggestive of a diffractive component. Similar results have been seen[11] for charged-charged, ++, --, and +- particle production in 205 GeV/c pp interactions at NAL. The value of the correlation function varies with the nature of the particles involved, $R(0, 0)$ being most positive in the central region for +- and less positive for the -- and ++ cases.

The constraints inherent for pp interactions are convenient in providing experimental checks on the data but limit the amount of information that can be extracted. In pp interactions the correlation functions and two-particle distributions must exhibit forward-backward symmetry about the diagonal $y_1 = -y_2$. Furthermore there must always be symmetry about the other diagonal, $y_1 = y_2$. As shown in Fig. 7, these symmetries need not be present in $\pi^- p$ interactions, and, while this reduces the number of constraints available in constructing plots, considerably more information is available in the plots. For production of particles whose nature is not distinguished there must be symmetry about the diagonal $y_1 = y_2$. For production of unlike particles no symmetry is required.

The contour plots of $R(y_1, y_2)$ which we present come from a study of a sample of completely reconstructed events of all multiplicities. Events of a given multiplicity are weighted so that the sum of the weights gives the proper partial cross section for that multiplicity. Values of $R(y_1, y_2)$ were calculated for square bins 0.8 units by 0.8 units in rapidity. Values were calculated for several positions of bin centers to reduce small-scale statistical fluctuations. Symmetry was imposed where it is required and smoothing of the contours was performed to remove variations which were not considered significant. While details of the contour plots may be changed as the sample is improved, major features of the plots are not expected to change significantly. A study of the magnitude of $R(y_1, y_2)$ as a function of the bin size showed little

significant change. The full range of c.m. rapidity which is kinematically possible for charged pions in 205 GeV/c $\pi^- p$ interactions is ± 4.9 units. Plots are shown for a y range of ± 3.6 units about the c.m. due to statistical limitations of the present sample of data.

In Fig. 8a is shown a contour plot of $R(y_1, y_2)$ for all charged particles from all interactions of the type $\pi^- p \rightarrow$ charge + charge + . . . Studies of samples with all two-prong interactions removed and with various cuts to eliminate elastic events showed little significant change in the central region. An inelastic cross section of 20.93 mb was assumed[12]. We observe positive short-range correlations in the central region comparable in magnitude to those observed in pp interactions. The value of $R(0,0)$ is $+0.55 \pm 0.05$ and $C(0,0) = +1.55$. The contours are clearly elongated parallel to the line $y_1 = y_2$. The maximum value of $R(y_1, y_2)$ is found not at the center of the plot, but shifted toward negative rapidities. The maximum value is about +0.6 at $y_1 = y_2 \approx -0.4$. Other features observable in the plot include increased separation of the contours for $y_1 \approx -y_2$ and a suggestion of positive correlations for particles with a very large rapidity separation. These features remain even if all two-prong events are removed from the sample. We would expect diffractive processes to contribute strongly in these regions of the plot.

The plot of $R(y_1, y_2)$ for $\pi^- p \rightarrow \pi^- + \pi^- + \ldots$ (with all negative particles assumed to be pions) is shown in Fig. 8b. Positive correlations in the central region are again seen. The value of $R(0,0)$ is $+0.32 \pm 0.07$, $C(0,0) = +0.23$, and the maximum value of $R \approx +0.5$ occurs again at

$y_1 = y_2 \approx -0.4$. The deviations from foward-backward symmetry are distinctly greater in this case, consistent with one of the incident particles being a π^-. Again, long-range correlations qualitatively consistent with diffractive contributions are observed, but they are shifted from the line $y_1 \approx -y_2$. In the reaction $\pi^- p \rightarrow \pi^+ + \pi^+ + \ldots$ shown in Fig. 8c (protons identified by bubble density[2] have been removed from the sample) there is even a suggestion of a double-peak in the central region, although the decrease in $R(y_1 = y_2)$ between the peaks is not statistically significant. We find $R(0,0) = +0.40 \pm 0.08$ and $C(0,0) = +0.28$. Maximum values of $R \approx +0.43$ occur at $y_1 = y_2 \approx -0.4$ and $y_1 = y_2 \approx +0.8$ and a value of $+0.36$ at $y_1 = y_2 \approx +0.4$. Again the contours are furthest apart for $y_1 \approx -y_2$ but, with the present statistics, no significant positive correlations are seen at the extremes. The contour plots for $\pi^-\pi^-$ and $\pi^+\pi^+$ are quite similar throughout much of the central region. The largest difference appears near the boundary where there appear to be long-range correlations in the $\pi^-\pi^-$ plot.

The correlation plot for $\pi^- p \rightarrow \pi^- + \pi^+ + \ldots$ seen in Fig. 8d shows positive correlations of even greater magnitude and the contours are even more elongated parallel to $y_1 = y_2$ and more closely spaced along $y_1 = -y_2$. There is no symmetry about either diagonal. The value of $R(0,0)$ is $+0.74 \pm 0.07$, $C(0,0) = +0.52$, and the maximum value of $R \approx +0.8$ is again shifted slightly from the center of the plot. Several suggestions are seen of structure at large rapidities which appear consistent with dissociation of projectile or target particle or of both.

The situation for 205 GeV/c $\pi^- p$ interactions can be compared with that at lower incident momenta. At 18.5 GeV/c, for example[13], an increase of the correlation functions in the central region is also seen. However, the maxima of $R(y_1, y_2)$ are considerably less positive in value when a corresponding normalization is used and the contours appear less elongated. At 8.05 GeV/c, $R(y_1, y_2)$ for $\pi^- p \rightarrow \pi^- + \pi^- + \ldots$ shows an increase in the central region but never assumes positive values.

The 205 GeV/c $\pi^- p$ double-differential invariant cross sections, $\pi^{-2} d\sigma/dy_1 dy_2$, are shown in Fig. 9 as functions of y_2 for various ranges of y_1. The correlation functions plotted in Fig. 8, have been calculated from these and from the corresponding single-particle distributions (see Fig. 4, for example). They may be examined for evidence of the short-range positive correlations seen in the plots of the correlation functions. At 18.5 GeV/c, plots of $d\sigma/dy_1 dy_2$ published by Notre Dame[13] clearly displayed the rapid decrease in cross section as c.m. rapidities become large. Also evident was a tendency for the maxima of the distributions to move toward negative y_2 as y_1 became more positive and toward positive y_2 as y_1 became more negative. This shift was consistent with what might be expected from momentum conservation when the total number of particles is relatively small. No clear plateau development was evident in either the single-particle or two-particle differential cross sections.

The two-particle distributions of Fig. 9 appear significantly broader than the corresponding distributions at 18.5 GeV/c. The magnitude of $\pi^{-2} d\sigma/dy_1 dy_2$ seems relatively constant in a range about $y_1 = y_2 = 0$ in

all cases. Thus a central plateau seems to be developing in the two-particle distributions as well as in the single-particle distributions. In the $\pi^+\pi^+$ case (Fig. 9c) the plateau seems to include the region with $|y_1|$ and $|y_2|$ both $\lesssim 1.6$ units of rapidity. In the distributions involving negative particles the plateau may be somewhat smaller and may be centered at somewhat positive values of y for the negative particles. The magnitude of the two-particle differential cross section in the central region seems to have increased significantly between 18.5 and 205 GeV/c. For example, in the reaction $\pi^- p \to \pi^- + \pi^- + \ldots$ at 205 GeV/c the maximum value of $\pi^{-2} d\sigma/dy_1 dy_2$ is about 2.3 mb, while at 18.5 GeV/c the maximum is about 1.3 mb.

The trend of the distributions to shift toward positive y_2 as y_1 becomes more negative and vice versa is much less pronounced than at lower energies. Instead, especially in the central region, the peaks of the distributions tend to move toward positive y_2 as y_1 becomes more positive and toward negative y_2 as y_1 becomes more negative. This tendency for particles to be closer together in rapidity than would be expected if they were uncorrelated is presumably responsible for the positive correlations seen in Fig. 8.

Within the central region the falloff of the correlation functions as a function of $\Delta y = y_2 - y_1$ appears reasonably consistent either with an exponential falloff of the form $\exp(-|\Delta y|/L)$ or with a gaussian of the form $\exp(-\Delta y^2/L^2)$. This is illustrated for the reaction $\pi^- p \to$ charge + charge + . . . in Fig. 10 where $R(y_1, y_2)$ is plotted as a function of Δy for fixed values of $(y_1 + y_2)$. Corresponding distributions for the other inclusive

reactions are generally similar in appearancc except for relatively slight asymmetries in the $\pi^-\pi^+$ case. The falloff appears consistent with a correlation length L of about 1.5 units of rapidity; we note however that if $R(y_1, y_2)$ is plotted as a function of Δy or of y_2 for fixed y_1 as other experimenters have sometimes done, the resulting asymmetric curves could be interpreted in terms of a correlation length about $\sqrt{2}$ times as large or ≈ 2 units.

Further information about the characteristics of multiparticle production processes may be obtained from a study of semi-inclusive correlation functions for fixed secondary-particle multiplicity n. The semi-inclusive correlation functions as a function of secondary charge multiplicity are defined as:

$$R^n(y_1, y_2) = \frac{\rho_2(y_1, y_2, n)}{\rho_1(y_1, n)\,\rho_1(y_2, n)} - 1$$

and $$C^n(y_1, y_2) = \rho_2(y_1, y_2, n) - \rho_1(y_1, n)\,\rho_1(y_2, n)$$

with $\rho_1(y,n) = \sigma_n^{-1} d\sigma/dy$ and $\rho_2(y_1, y_2, n) = \sigma_n^{-1} d\sigma/dy_1, dy_2$ where σ_n is the cross section for producing n charged particles. In Table I are shown our results for $R^n(0,0)$ and $C^n(0,0)$ as a function of n for $4 \leqslant n \leqslant 14$. Values are given for charge-charge, --, ++, and -+ correlations. In general the semi-inclusive correlation functions have values much less positive than those exhibited by the inclusive correlation functions in the central region. For $R^n_{cc}(0,0)$ we observe values consistent with zero for $4 \leqslant n \leqslant 14$; only $R^4_{cc}(0,0)$ is positive. The values of $R^n_{--}(0,0)$ and $R^n_{++}(0,0)$ are all negative. Only the $R^n_{-+}(0,0)$ values are positive and

only $R^4_{-+}(0,0)$ is comparable in magnitude to the positive correlations observed in the central region for the inclusive reactions.

Our results may be compared with results for pp collisions at ISR and NAL energies. In the Pisa-Stony Brook experiment[14] at the ISR, positive values of $R^n_{cc}(\eta_1 = 0, \eta_2 = 0)$ have been reported for all values of n. For pp collisions at 205 GeV/c, Singer et. al.[15] found $R^n_{cc}(0,0)$ to be within two standard deviations of zero for all n, consistent with our findings. They also found negative values of $R^n_{--}(0,0)$ and $R^n_{++}(0,0)$ for all multiplicities. Positive values for $R^n_{-+}(0,0)$ were found; the values were largest and most significant for $n = 4$ and 6, and evidence was presented to associate these correlations with diffractive-type events. A detailed comparison of Table I with these data suggests that the semi-inclusive rapidity correlations in $\pi^- p$ interactions at 205 GeV/c are quite similar to those in pp interactions at the same energy.

In summary short-range positive rapidity correlations are observed in charge-charge $\pi^-\pi^-$, $\pi^+\pi^+$, and $\pi^-\pi^+$ two-particle inclusive reactions at 205 GeV/c It is hoped that further study will provide information about the mechanism producing these correlations and about the dynamical processes involved in multiparticle production.

FOOTNOTES AND REFERENCES

*Supported in part by the National Science Foundation, the U.S. Atomic Energy Commission, and the National Research Council of Canada.

1. We wish to express our appreciation to the members of the NAL-Berkeley Exp. 137 Collaboration for providing us with the bubble chamber film from this run after ~6 months.
2. All negative tracks in the sample were assumed to be π^- mesons. Protons with $p_{lab} < 1.3$ GeV/c were identified by ionization. All other positive particles have been treated as π^+ mesons. No corrections for charged K-mesons or for fast protons have been made at this stage in the analysis.
3. In the present sample, 6% of negative tracks with momenta from spark-chamber "hookup" corresponding to $x > +0.2$ were in the $x > +1.0$ range as compared to 16% of all tracks with $x > +0.2$ when only bubble-chamber measurements were used. The corresponding percentages for positive tracks were 5% and 12%, respectively.
4. J.T. Powers et. al., Phys. Rev. D8, 1947 (1973).
5. Alma-Ata, Bucharest, Budapest, Cracow, Dubna, Hanoi, Serpukhov, Sofia, Tashkent, Tbilisi, Ulan-Bator, Warsaw Collaboration, Proceedings of the IInd Aix-en-Provence International Conference on Elementary Particles, 1973 (to be published).
6. Arguments for factorization are summarized in a thesis by H. I. Miettinen, University of Helsinki (1973). See also H. I. Miettinen, Phys. Lett. 38B, 473 (1972).

7. Argonne-Iowa State-Maryland-NAL-Michigan State paper, submitted to the Berkeley meeting of the DPF, American Physical Society, 13-17 August, 1973.

8. Berkeley-Notre Dame Collaboration, M. Alston-Garnjost et. al., Phys. Letters 39B, 402 (1972).

9. H. Dibon et. al., Phys. Letters 44B, 313 (1973).

10. S.R. Amendolia, et. al., Phys. Letters 48B, 359 (1974).

11. R. Singer et. al., "Inclusive Two-Particle Rapidity Correlations in 205 GeV/c pp Interactions," Argonne Report No. NAL/HEP 7368 (December, 1973).

12. D. Bogert et. al., Phys. Rev. Letters 31, 1271 (1973).

13. W.D. Shephard et. al., Phys. Rev. Letters 28, 703 (1973).

14. G. Bellettini, "Results from the Pisa-Stony Brook ISR Experiment," High Energy Collisions-1973 (Stony Brook), AIP Conference Proceedings Number 15 (C. Quigg, Editor), p. 9.

15. R. Singer et. al., "Semi-Inclusive Two-Particle Rapidity Correlations in 205 GeV/c pp Interactions," Argonne Report No. NAL/HEP 7369 (December, 1973).

Table I

Values of the Semi-Inclusive Rapidity Correlation Functions $R(0,0,n)$ and $C(0,0,n)$

n	$R^n_{cc}(0,0)$	$C^n_{cc}(0,0$	$R^n_{--}(0,0)$	$C^n_{--}(0,0)$	$R^n_{++}(0,0)$	$C^n_{++}(0,0)$	$R^n_{-+}(0,0)$	$C^n_{-+}(0,0)$
4	+0.25 ± 0.23	+0.05	-0.14 ± 0.31	-0.01	-0.42 ± 0.22	-0.02	+0.81 ± 0.43	+0.04
6	-0.07 ± 0.10	-0.06	-0.18 ± 0.15	-0.04	-0.53 ± 0.10	-0.11	+0.21 ± 0.17	+0.05
8	-0.01 ± 0.08	-0.03	-0.27 ± 0.10	-0.15	-0.25 ± 0.10	-0.14	+0.23 ± 0.12	+0.13
10	-0.02 ± 0.08	-0.08	-0.18 ± 0.10	-0.23	-0.18 ± 0.10	-0.19	+0.15 ± 0.11	+0.17
12	-0.03 ± 0.08	-0.23	-0.16 ± 0.10	-0.36	-0.13 ± 0.11	-0.29	+0.09 ± 0.10	+0.21
14	-0.03 ± 0.10	-0.41	-0.15 ± 0.18	-0.60	-0.03 ± 0.15	-0.11	+0.04 ± 0.12	+0.15

FIGURE CAPTIONS

Fig. 1. (a) Experimental arrangement for NAL Exp. 2B, 205 GeV/c $\pi^- p \to \pi^\pm + \ldots$

(b) Measuring error $\Delta p/p$ as a function of p_{lab} for measurements with bubble chamber alone (x) and combined bubble chamber-wide gap chamber hybrid spectrometer (⊙) measurements.

Fig. 2. Distribution of the invariant structure function $(2E/\pi\sqrt{s})\, d\sigma/dx$ as a function of the Feynman x variable for (a) final-state π^- and (b) final-state π^+. The superimposed "x" points for large positive x represent an alternate distribution of tracks with measured momenta corresponding to $x > 1.0$ as described in the text. Distributions for lower-energy data are shown for comparison.

Fig. 3. Distributions of $d\sigma/dp_T^2$ as a function of p_T^2 for (a) final-state π^- and (b) final-state π^+.

Fig. 4. Distributions of the invariant structure function $\pi^{-1} d\sigma/dy$ as a function of c.m. rapidity y for (a) final-state π^- and (b) final-state π^+. Distributions for lower-energy data are shown for comparison.

Fig. 5. (a) C.m. rapidity distributions for π^- from 205 GeV/c $\pi^- p$ and pp interactions obtained with the same experimental arrangement, normalized to the same total cross section as a test of factorization in the target fragmentation region.

(b) Rapidity distributions for π^- from $\pi^- p$ interactions at 205 GeV/c, 40 GeV/c and 18.5 GeV/c. The distributions for 40 GeV/c and 18.5 GeV/c have been boosted to the laboratory rest frame for the 205 GeV/c distribution (see upper scale) to allow a comparison of the target proton fragmentation to π^-.

Fig. 6. Plots showing the approach to scaling for (a) the central region and (b) the target fragmentation region in $\pi^{\pm} p$ interactions. Data from 3.7 GeV/c to 205 GeV/c are shown.

Fig. 7. Axes of symmetry which must exist in plots of $R(y_1, y_2)$ as a function of y_1 and y_2 are shown for: (a) pp interactions involving production of like or unlike particles; (b) $\pi^- p$ interactions involving production of like particles (charged-charged, ++, --, etc); and (c) $\pi^- p$ interactions involving productions of unlike particles (e.g. +-).

Fig. 8. Contour plots showing lines of constant of $R(y_1, y_2)$ as a function of y_1 and y_2 for the two-particle inclusive reactions at 205 GeV/c: (a) $\pi^- p \rightarrow$ charge + charge + . . . (b) $\pi^- p \rightarrow \pi^- + \pi^-$ . . .; (c) $\pi^- p \rightarrow \pi^+ + \pi^+ + \ldots$; and (d) $\pi^- p \rightarrow \pi^- + \pi^+ + \ldots$

Fig. 9. Distributions of $\pi^{-2} d\sigma/dy_1 dy_2$ as a function of y_2 for various ranges of y_1 in the two-particle inclusive reactions at 205 GeV/c: (a) $\pi^- p \rightarrow$ charge + charge + . . .; (b) $\pi^- p \rightarrow \pi^- + \pi^- + \ldots$; (c) $\pi^- p \rightarrow \pi^+ + \pi^+ + \ldots$; (d) $\pi^- p \rightarrow \pi^- + \pi^+ + \ldots$ Various ranges of y_1 are indicated by different symbols as shown on

the figure. The lines connecting the points are included to make it easier to follow the trend of the data.

Fig. 10. Distributions of $R(y_1, y_2)$ as a function of $\Delta y = y_2 - y_1$ for fixed ranges of $(y_1 + y_2)$ in the central region for the two-particle inclusive reaction $\pi^- p \rightarrow$ charge + charge +. . . at 205 GeV/c.

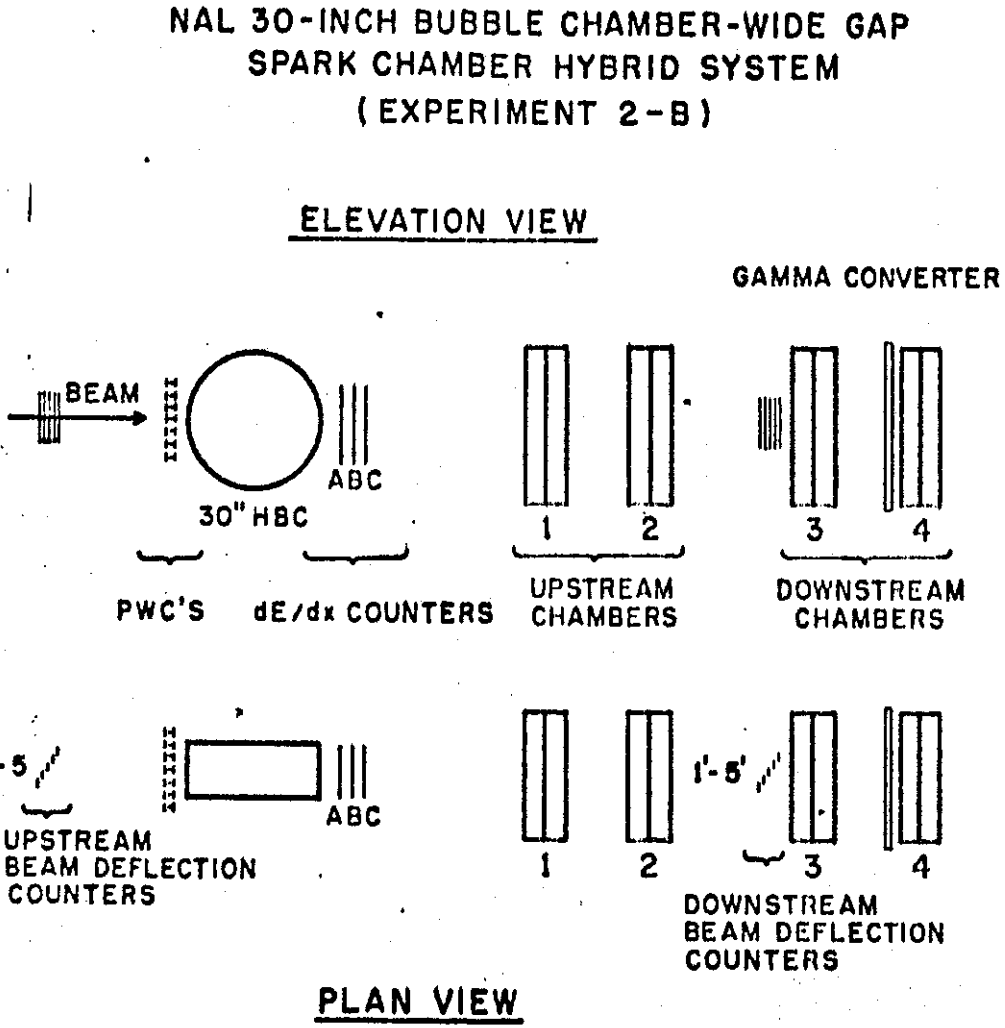
NAL 30-INCH BUBBLE CHAMBER-WIDE GAP
SPARK CHAMBER HYBRID SYSTEM
(EXPERIMENT 2-B)
ELEVATION VIEW
GAMMA CONVERTER
BEAM
ABC
30" HBC
1
2
3
4
PWC'S
dE/dx COUNTERS
UPSTREAM CHAMBERS
DOWNSTREAM CHAMBERS
-5
ABC
1'-5'
UPSTREAM BEAM DEFLECTION COUNTERS
DOWNSTREAM BEAM DEFLECTION COUNTERS
PLAN VIEW

Fig. 1a

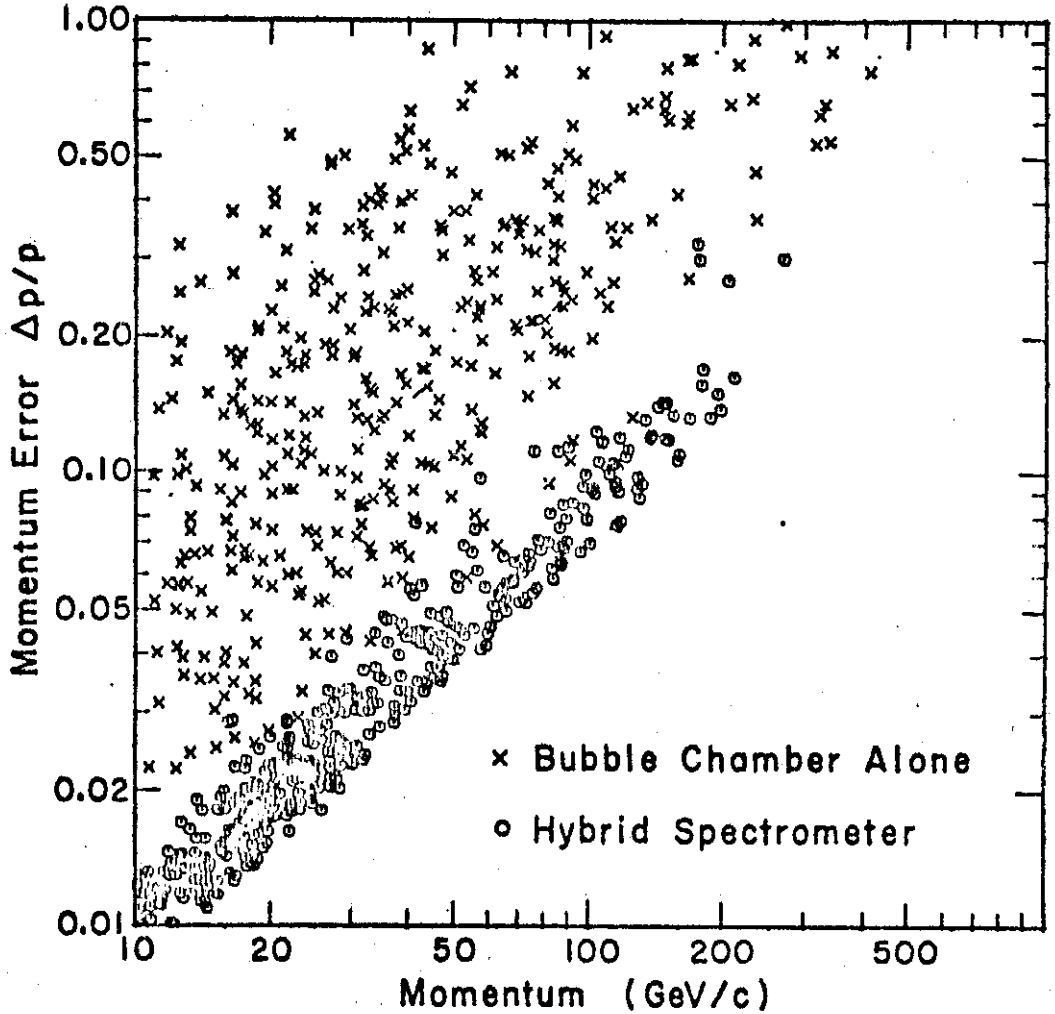
Momentum Error Δp/p
1.00
0.50
0.20
0.10
0.05
0.02
0.01
10
20
50
100
200
500
Momentum (GeV/c)
× Bubble Chamber Alone
○ Hybrid Spectrometer

Fig. 1b

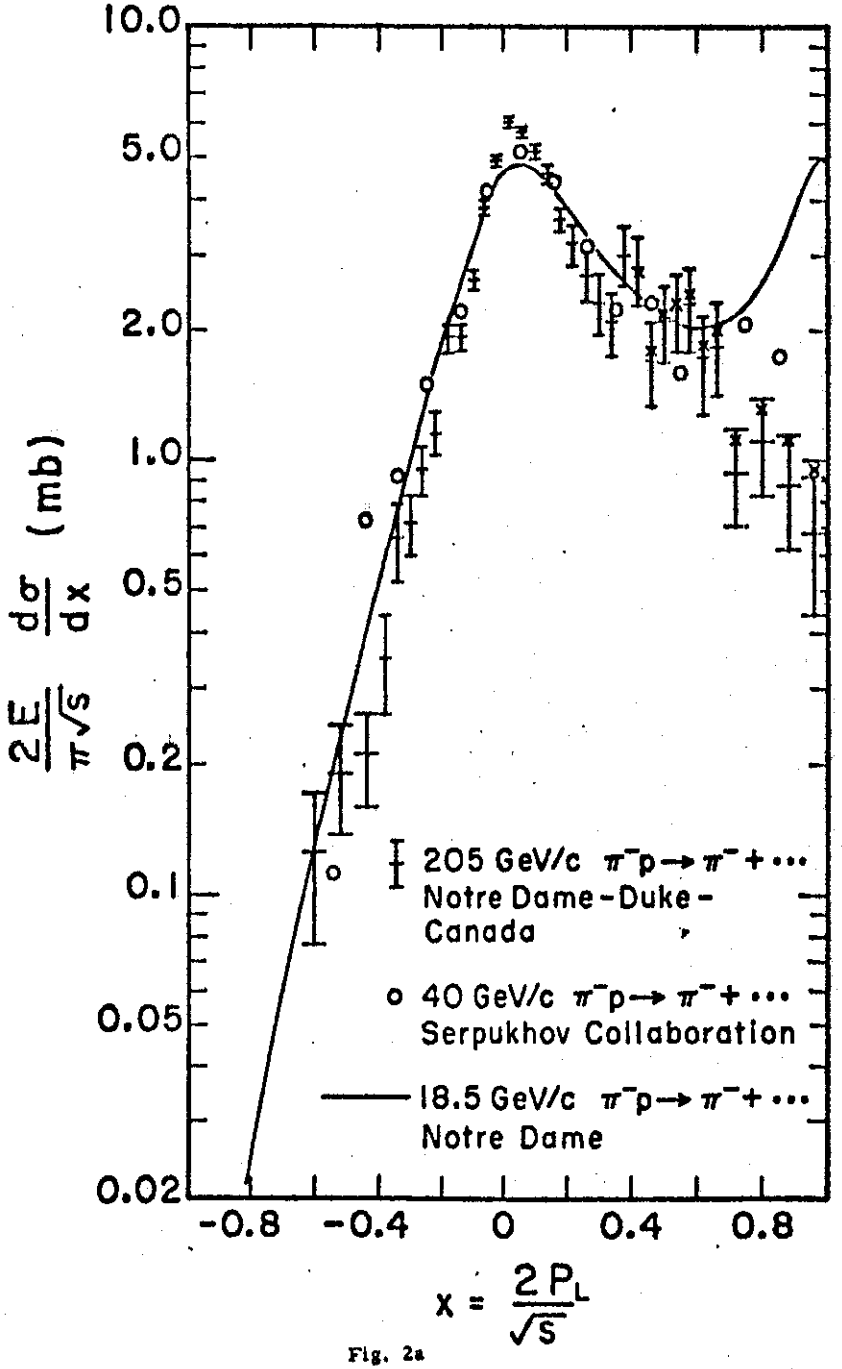
10.0
5.0
2.0
1.0
0.5
0.2
0.1
0.05
0.02
-0.8
-0.4
0
0.4
0.8
$\frac{2E}{\pi\sqrt{s}}\frac{d\sigma}{dx}$ (mb)
$x = \frac{2P_L}{\sqrt{s}}$
205 GeV/c $\pi^- p \to \pi^- + \cdots$
Notre Dame-Duke-Canada
40 GeV/c $\pi^- p \to \pi^- + \cdots$
Serpukhov Collaboration
18.5 GeV/c $\pi^- p \to \pi^- + \cdots$
Notre Dame

Fig. 2a

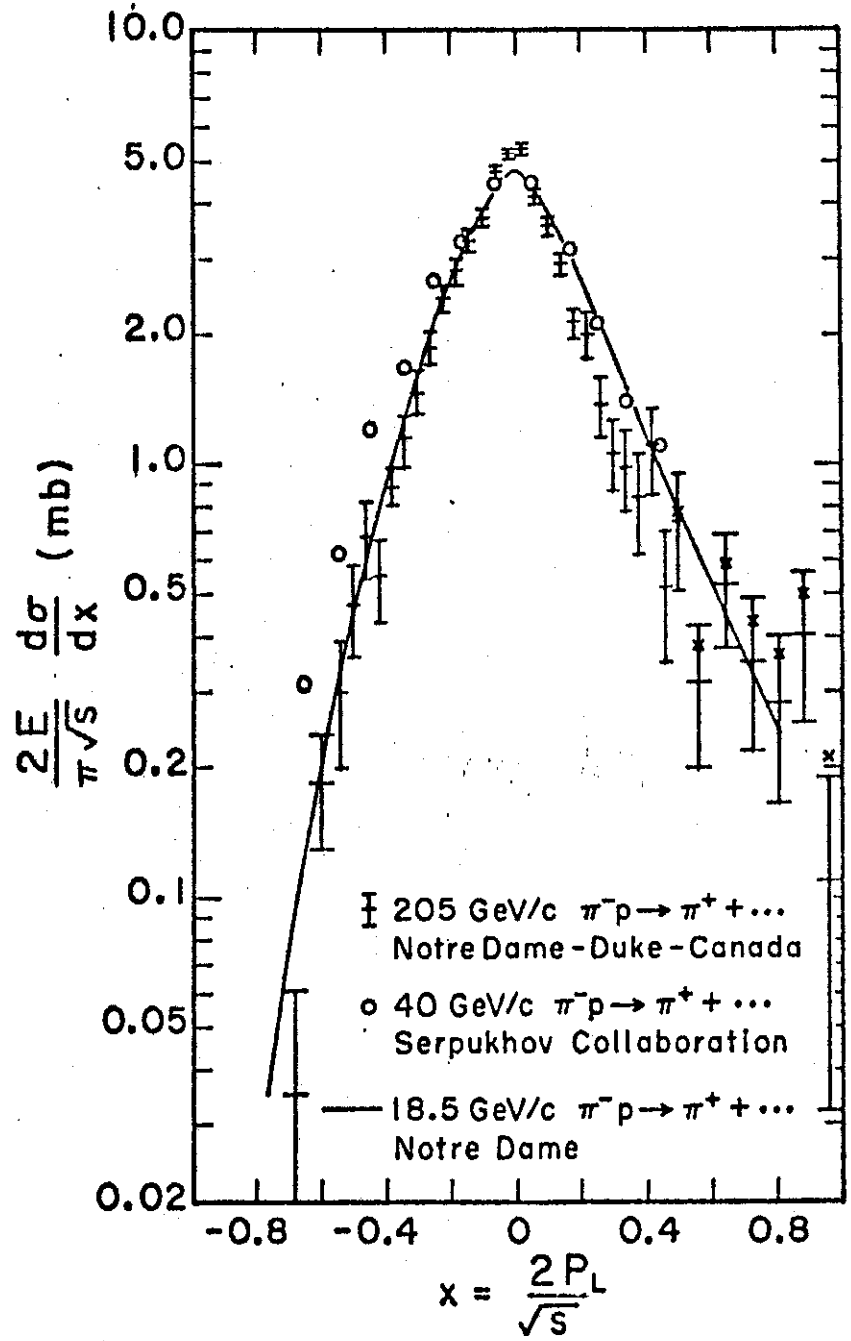
10.0
5.0
2.0
1.0
0.5
0.2
0.1
0.05
0.02
-0.8
-0.4
0
0.4
0.8
$\frac{2E}{\pi\sqrt{s}}\frac{d\sigma}{dx}$ (mb)
$x = \frac{2P_L}{\sqrt{s}}$
205 GeV/c $\pi^- p \to \pi^+ + \cdots$
Notre Dame-Duke-Canada
40 GeV/c $\pi^- p \to \pi^+ + \cdots$
Serpukhov Collaboration
18.5 GeV/c $\pi^- p \to \pi^+ + \cdots$
Notre Dame

Fig. 2b

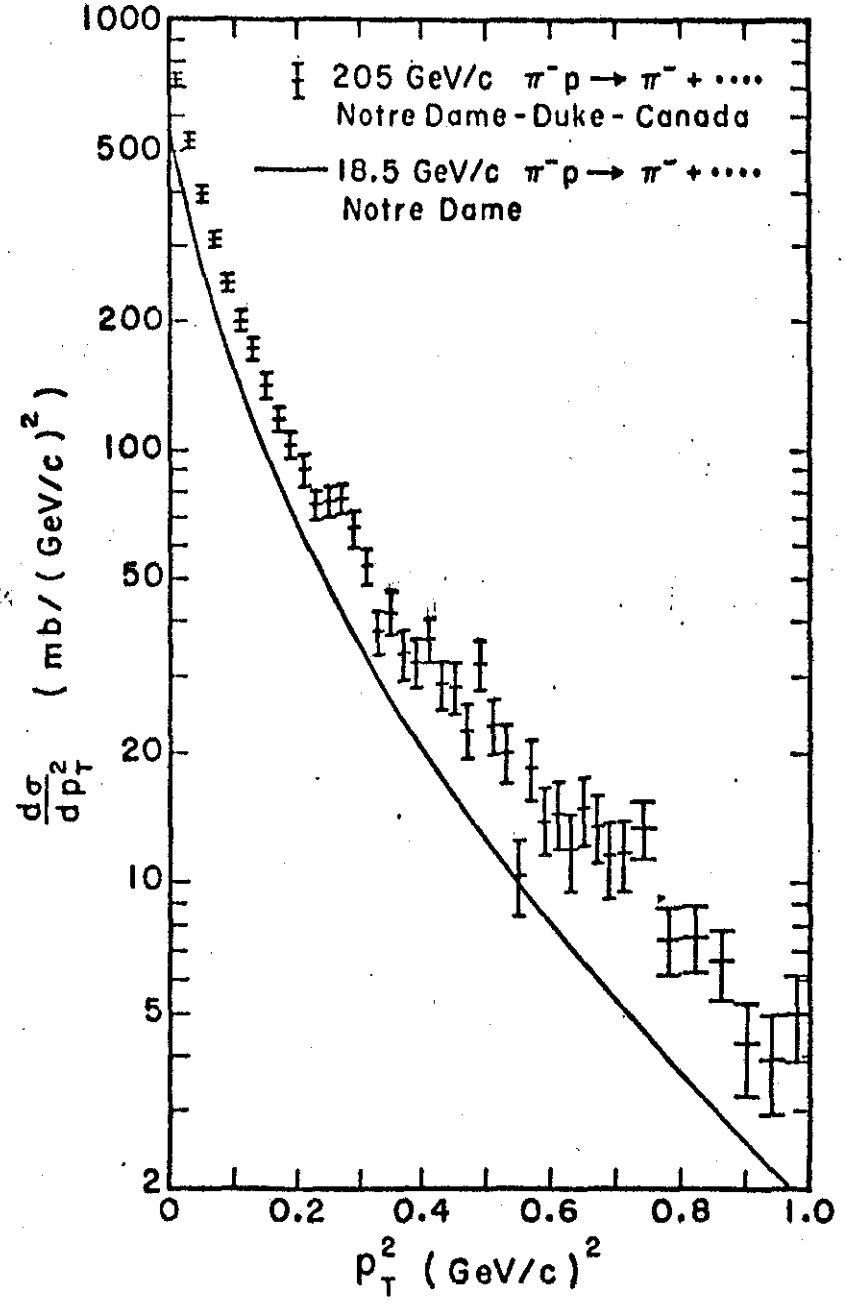
205 GeV/c $\pi^- p \rightarrow \pi^- + \cdots$
Notre Dame - Duke - Canada
18.5 GeV/c $\pi^- p \rightarrow \pi^- + \cdots$
Notre Dame
$\frac{d\sigma}{dp_T^2}$ (mb / (GeV/c)^2)
p_T^2 (GeV/c)^2
1000
500
200
100
50
20
10
5
2
0
0.2
0.4
0.6
0.8
1.0

Fig. 3a

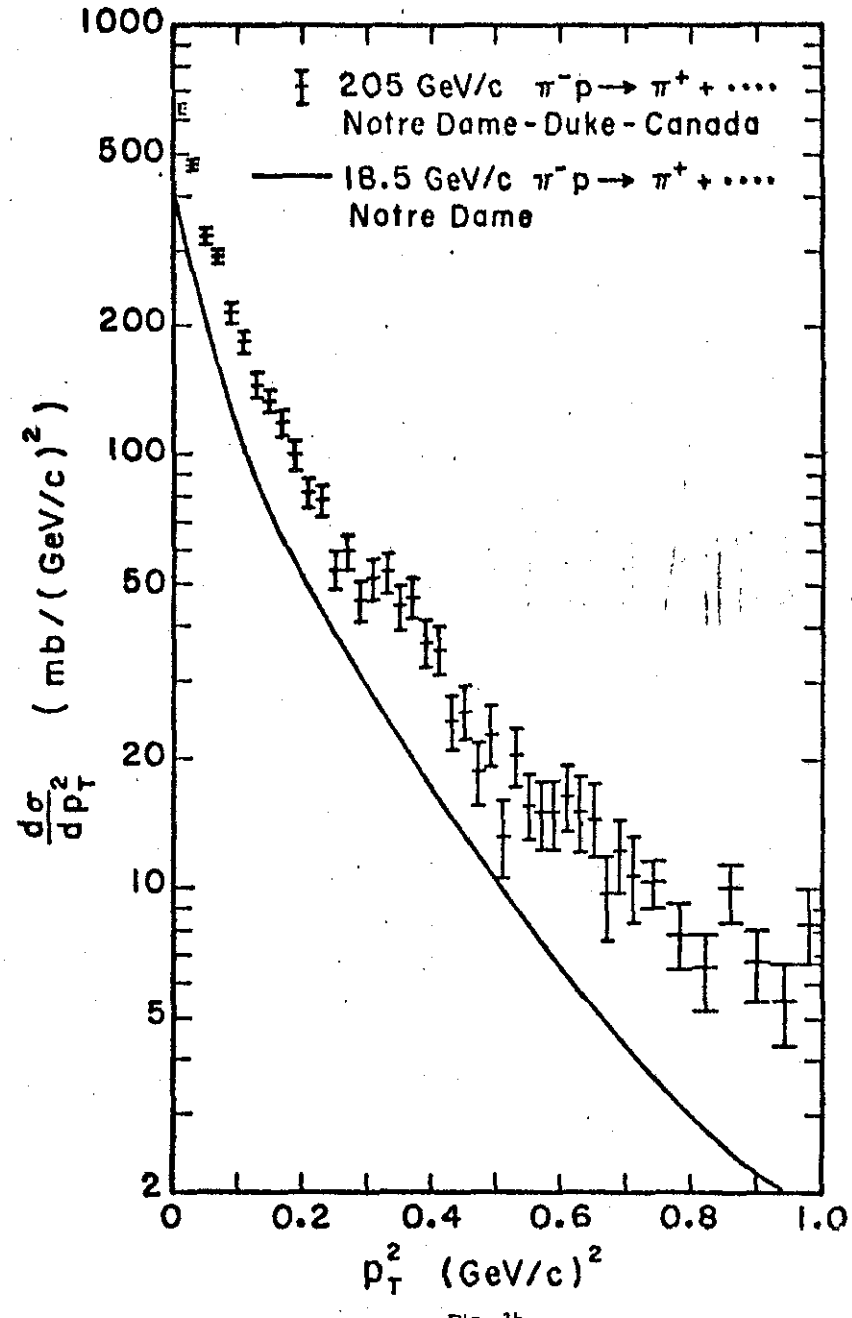
205 GeV/c $\pi^- p \rightarrow \pi^+ + \cdots$
Notre Dame - Duke - Canada
18.5 GeV/c $\pi^- p \rightarrow \pi^+ + \cdots$
Notre Dame
$\frac{d\sigma}{dp_T^2}$ (mb / (GeV/c)^2)
p_T^2 (GeV/c)^2
1000
500
200
100
50
20
10
5
2
0
0.2
0.4
0.6
0.8
1.0

Fig. 3b

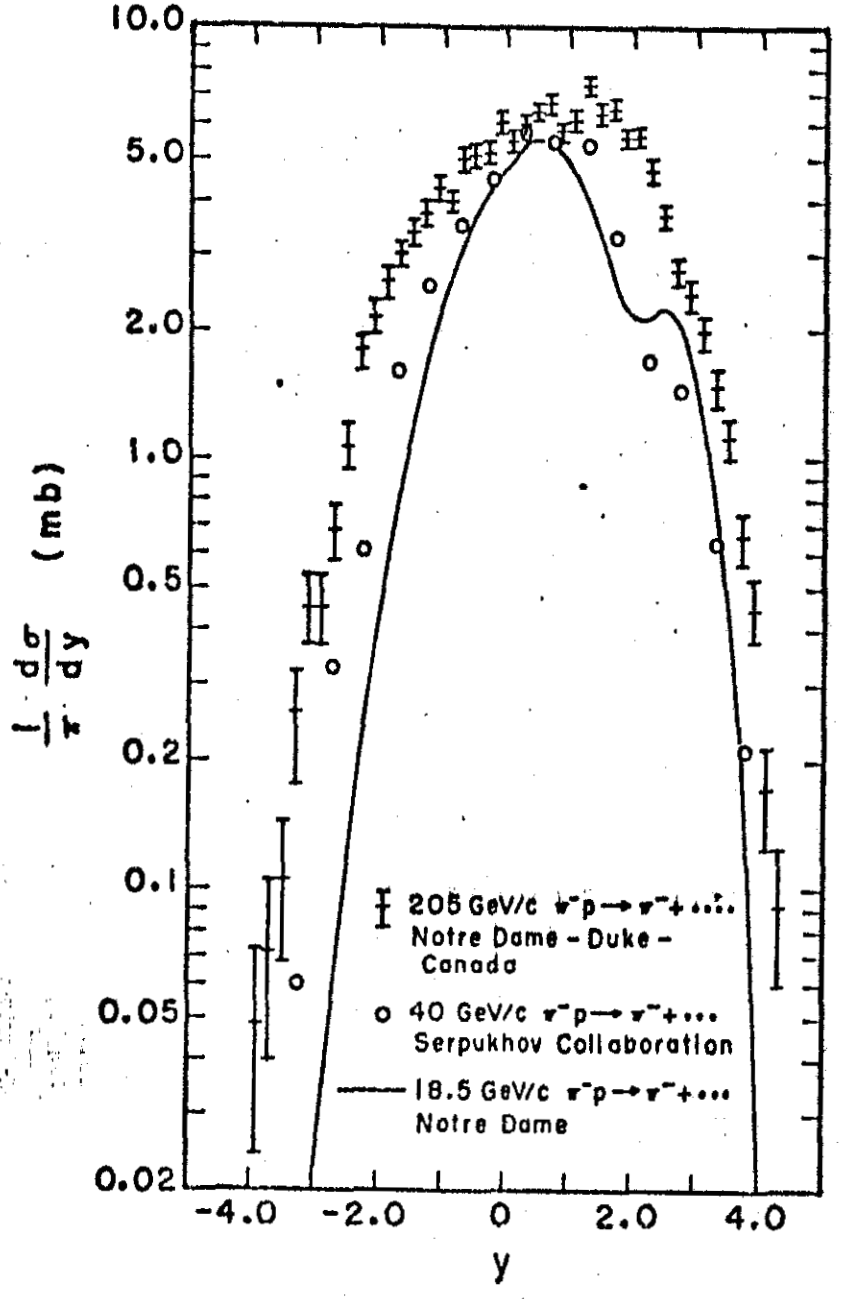
10.0
5.0
2.0
1.0
0.5
0.2
0.1
0.05
0.02
$\frac{1}{\pi}\frac{d\sigma}{dy}$ (mb)
-4.0
-2.0
0
2.0
4.0
y
205 GeV/c $\pi^- p \to \pi^- + \ldots$
Notre Dame - Duke - Canada
40 GeV/c $\pi^- p \to \pi^- + \ldots$
Serpukhov Collaboration
18.5 GeV/c $\pi^- p \to \pi^- + \ldots$
Notre Dame

Fig. 4a

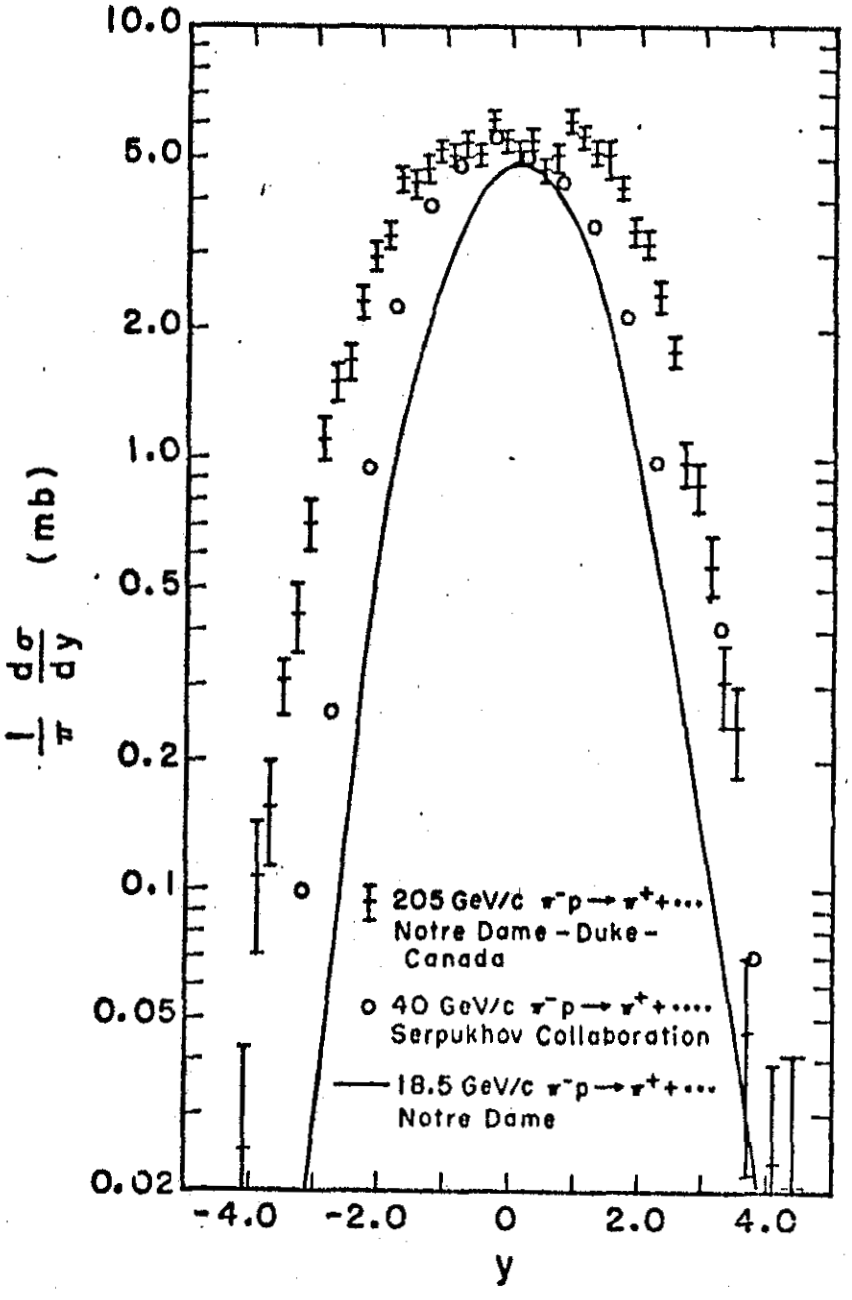
10.0
5.0
2.0
1.0
0.5
0.2
0.1
0.05
0.02
$\frac{1}{\pi}\frac{d\sigma}{dy}$ (mb)
-4.0
-2.0
0
2.0
4.0
y
205 GeV/c $\pi^- p \to \pi^+ + \ldots$
Notre Dame - Duke - Canada
40 GeV/c $\pi^- p \to \pi^+ + \ldots$
Serpukhov Collaboration
18.5 GeV/c $\pi^- p \to \pi^+ + \ldots$
Notre Dame

Fig. 4b

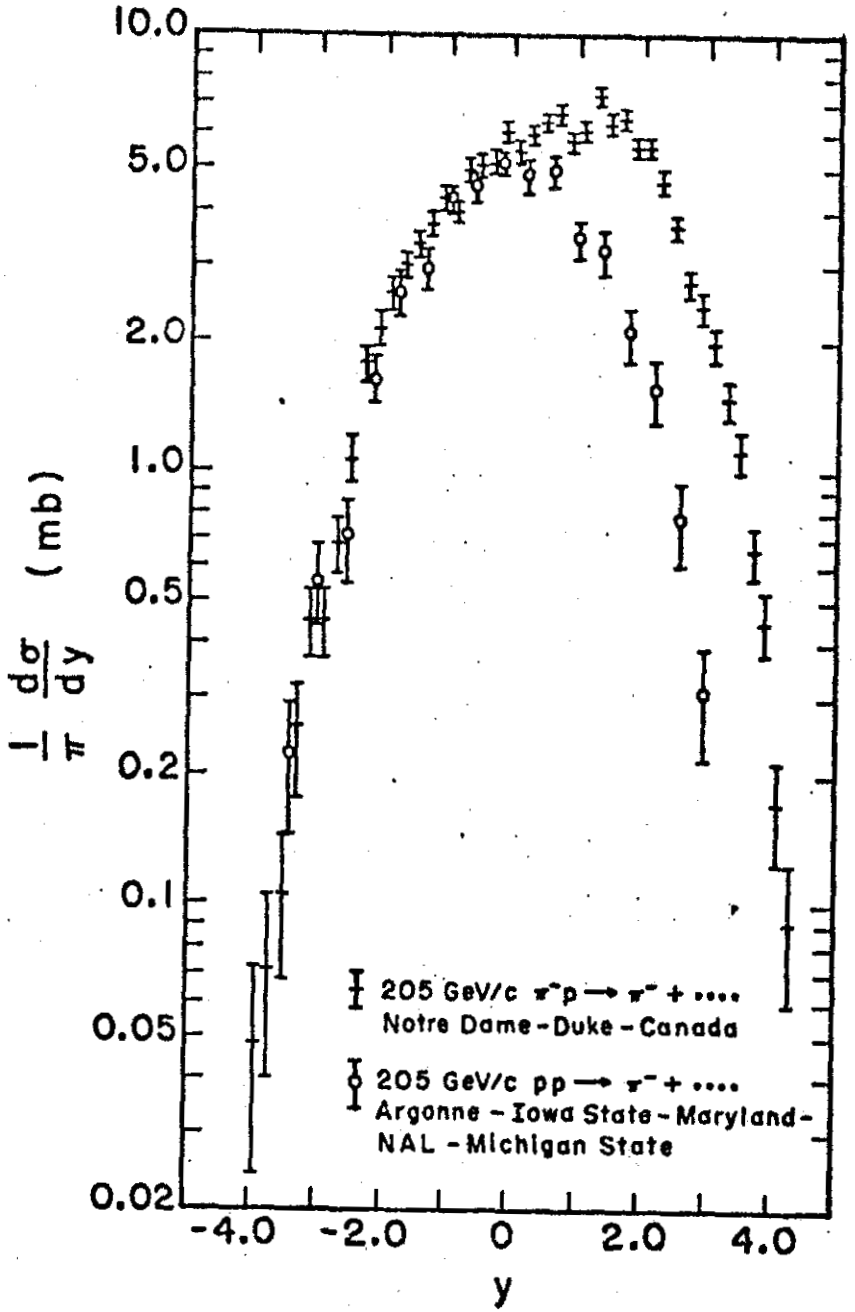
10.0
5.0
2.0
1.0
0.5
0.2
0.1
0.05
0.02
$\frac{1}{\pi}\frac{d\sigma}{dy}$ (mb)
-4.0
-2.0
0
2.0
4.0
y
205 GeV/c $\pi^- p \rightarrow \pi^- + \cdots$
Notre Dame - Duke - Canada
205 GeV/c $pp \rightarrow \pi^- + \cdots$
Argonne - Iowa State - Maryland - NAL - Michigan State

Fig. 5a

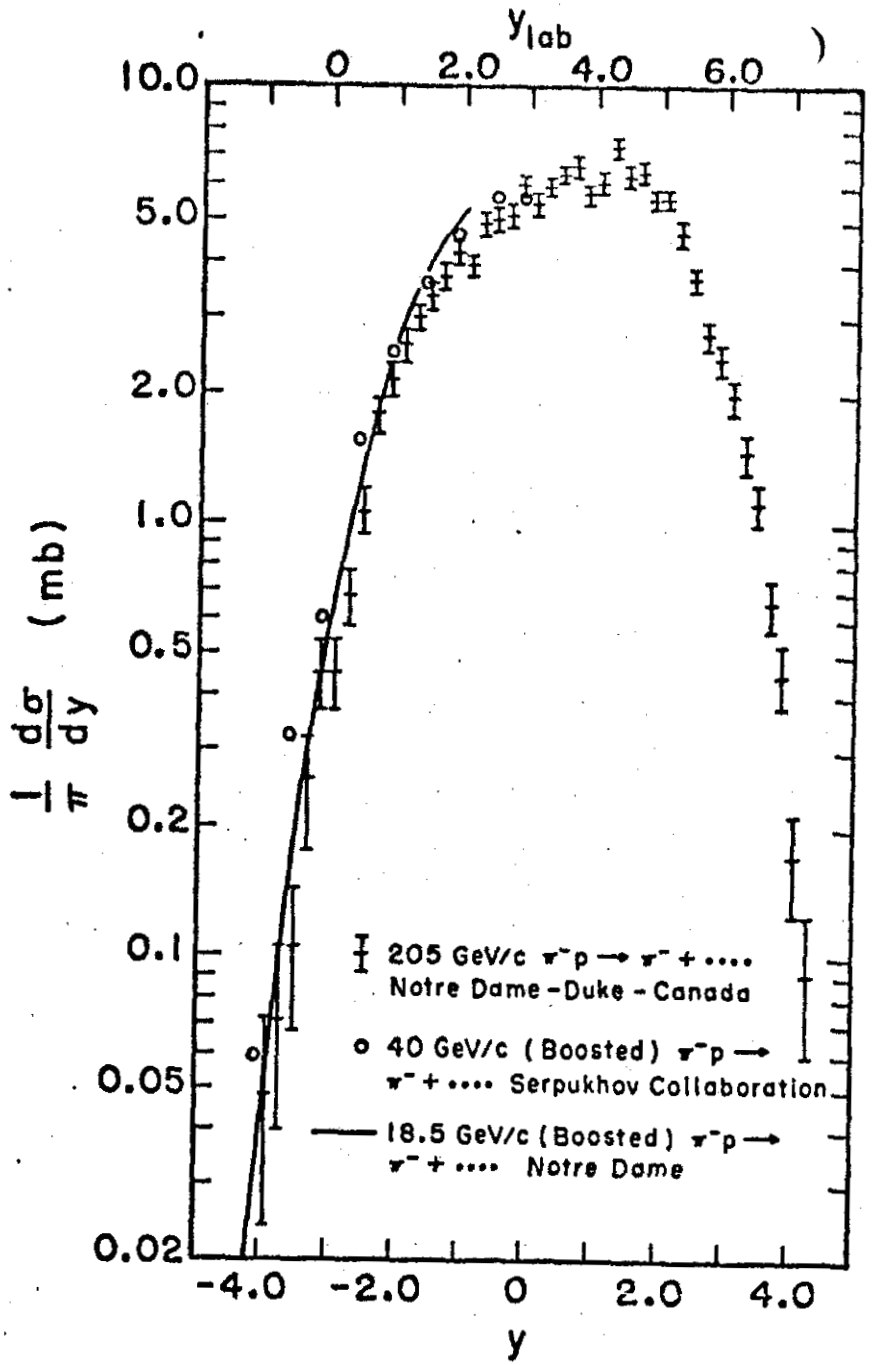
y_{lab}
0
2.0
4.0
6.0
10.0
5.0
2.0
1.0
0.5
0.2
0.1
0.05
0.02
$\frac{1}{\pi}\frac{d\sigma}{dy}$ (mb)
-4.0
-2.0
0
2.0
4.0
y
205 GeV/c $\pi^- p \rightarrow \pi^- + \cdots$
Notre Dame - Duke - Canada
40 GeV/c (Boosted) $\pi^- p \rightarrow \pi^- + \cdots$ Serpukhov Collaboration
18.5 GeV/c (Boosted) $\pi^- p \rightarrow \pi^- + \cdots$ Notre Dame

Fig. 5b

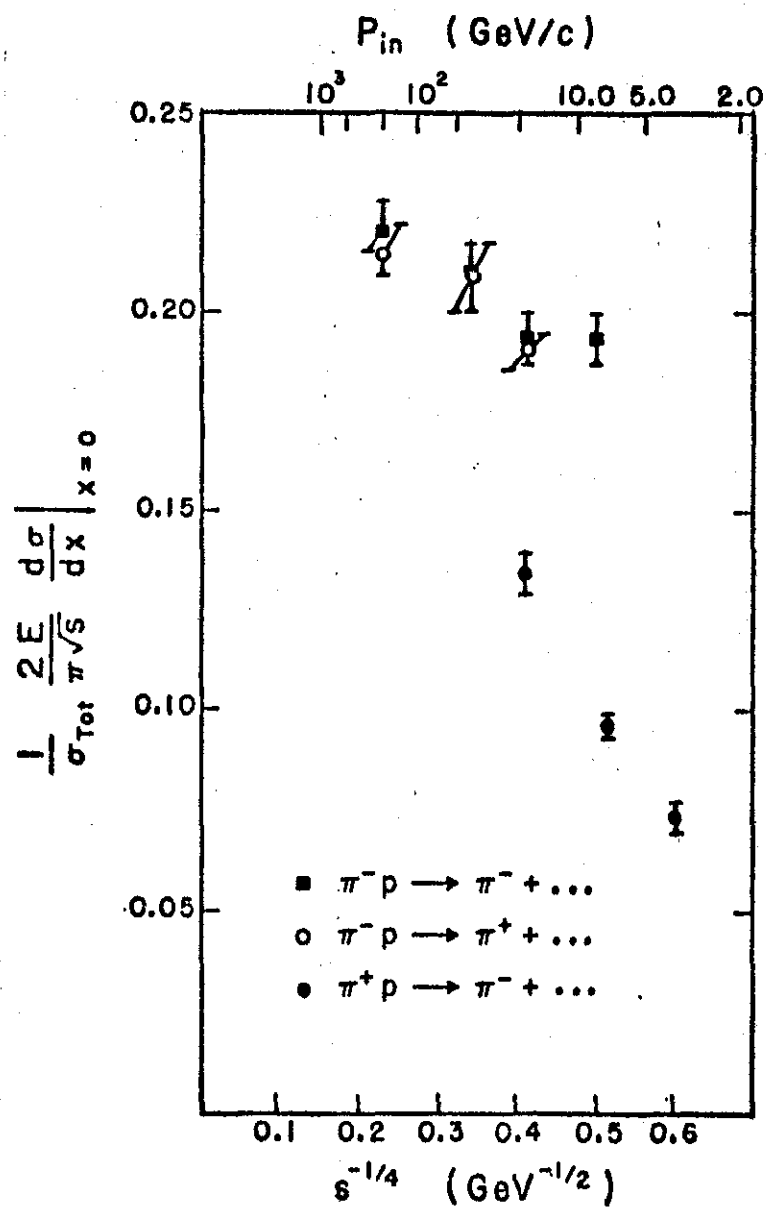
P_{in} (GeV/c)
10^3 10^2 10.0 5.0 2.0
0.25
0.20
0.15
0.10
0.05
$\frac{1}{\sigma_{Tot}} \frac{2E}{\pi\sqrt{s}} \frac{d\sigma}{dx}\Big|_{x=0}$
■ $\pi^- p \rightarrow \pi^- + \ldots$
○ $\pi^- p \rightarrow \pi^+ + \ldots$
● $\pi^+ p \rightarrow \pi^- + \ldots$
0.1 0.2 0.3 0.4 0.5 0.6
$s^{-1/4}$ ($GeV^{-1/2}$)

Fig. 6a

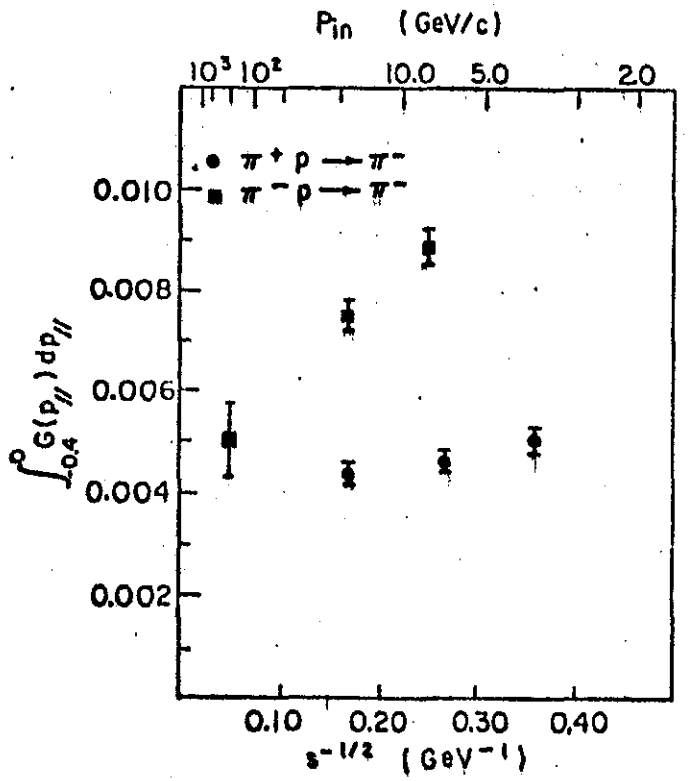
P_{in} (GeV/c)
10^3 10^2 10.0 5.0 2.0
● $\pi^+ p \rightarrow \pi^-$
■ $\pi^- p \rightarrow \pi^-$
0.010
0.008
0.006
0.004
0.002
$\int_{0.4}^{0} G(p_{//})\, dp_{//}$
0.10 0.20 0.30 0.40
$s^{-1/2}$ (GeV^{-1})

Fig. 6b

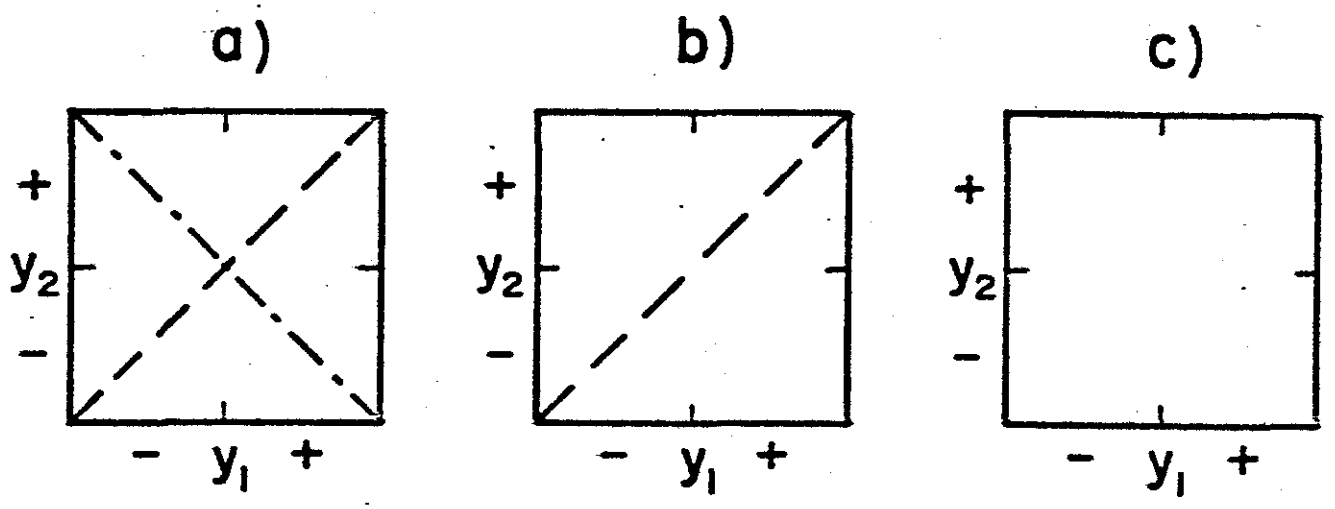

Fig. 7

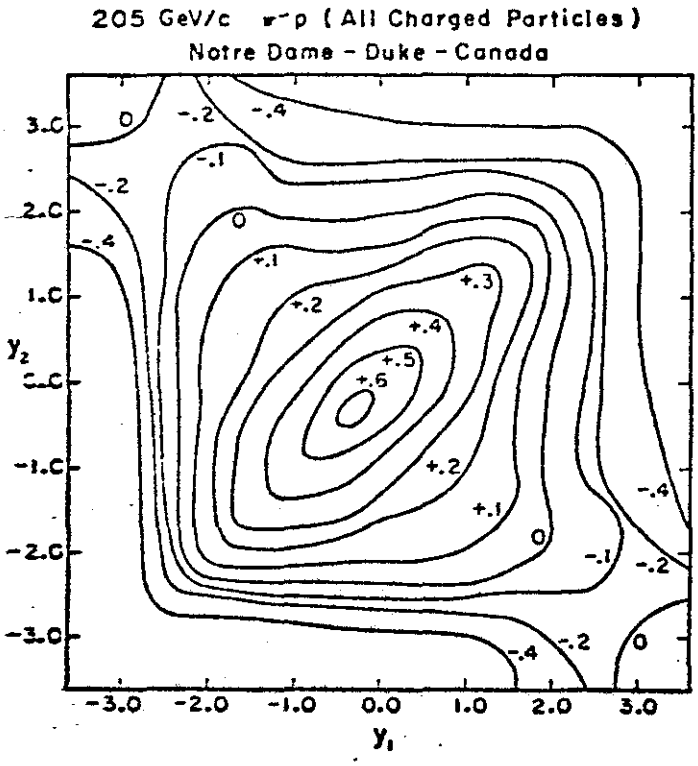

Fig. 8a

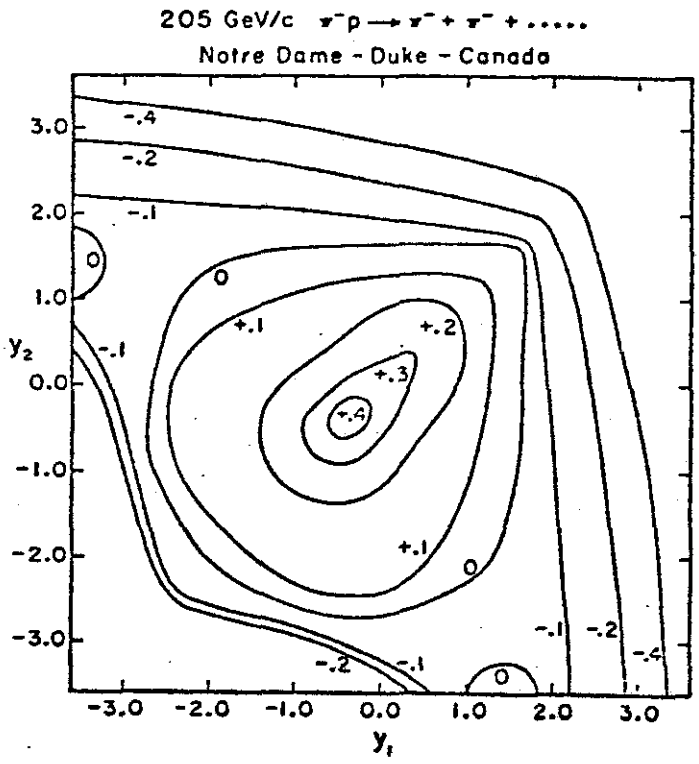

Fig. 8b

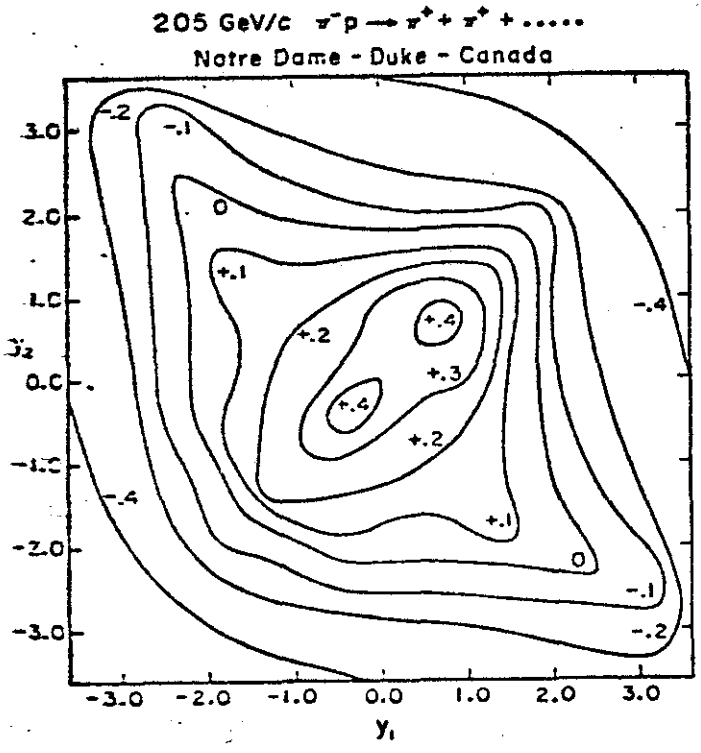

Fig. 8c

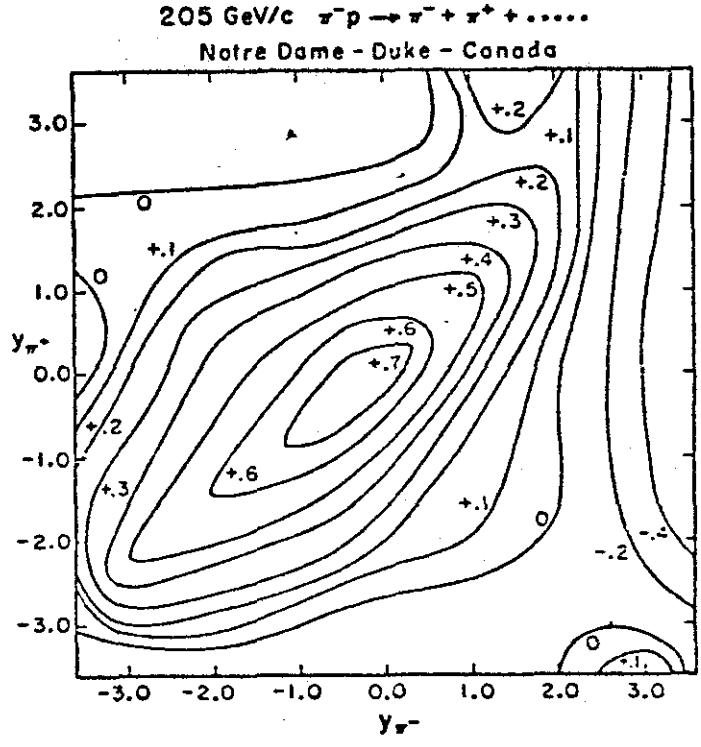

Fig. 8d

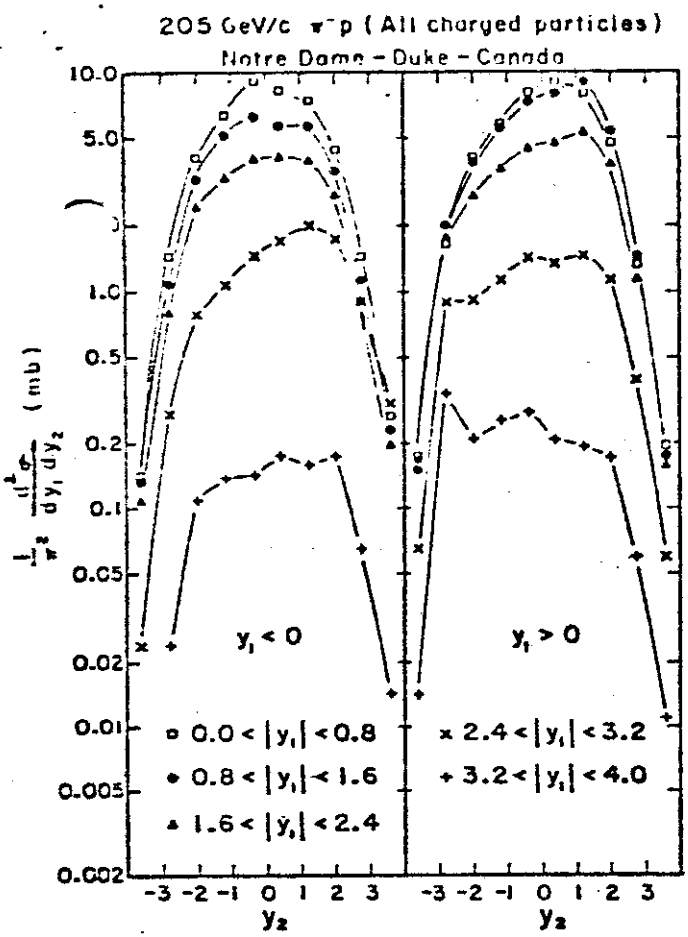

Fig. 9a

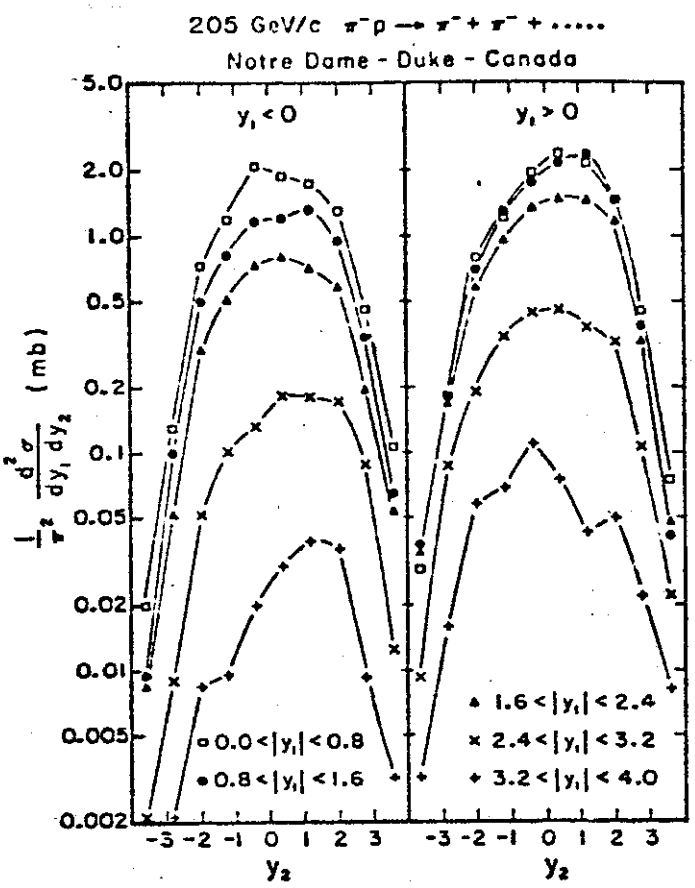

Fig. 9b

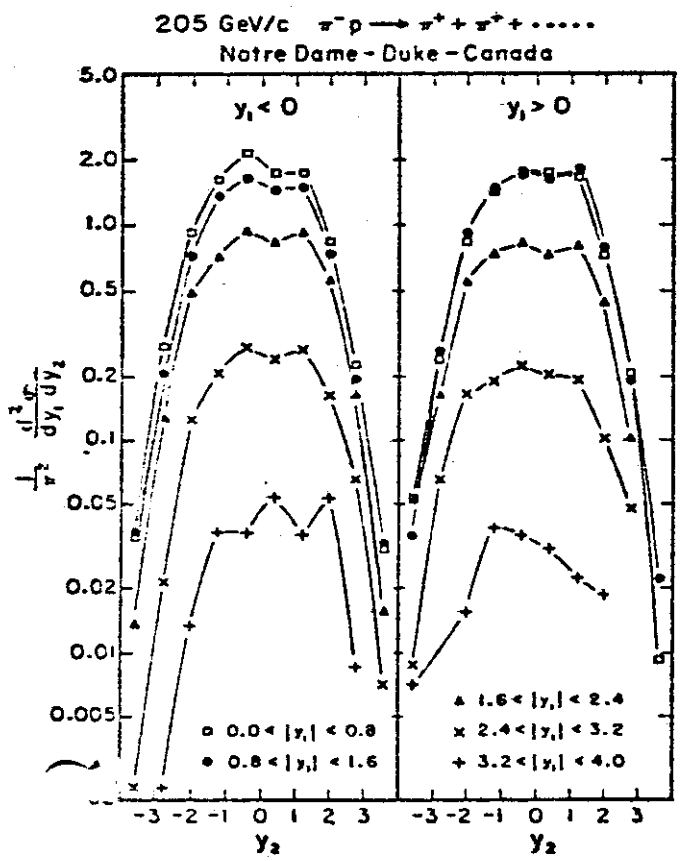

Fig. 9c

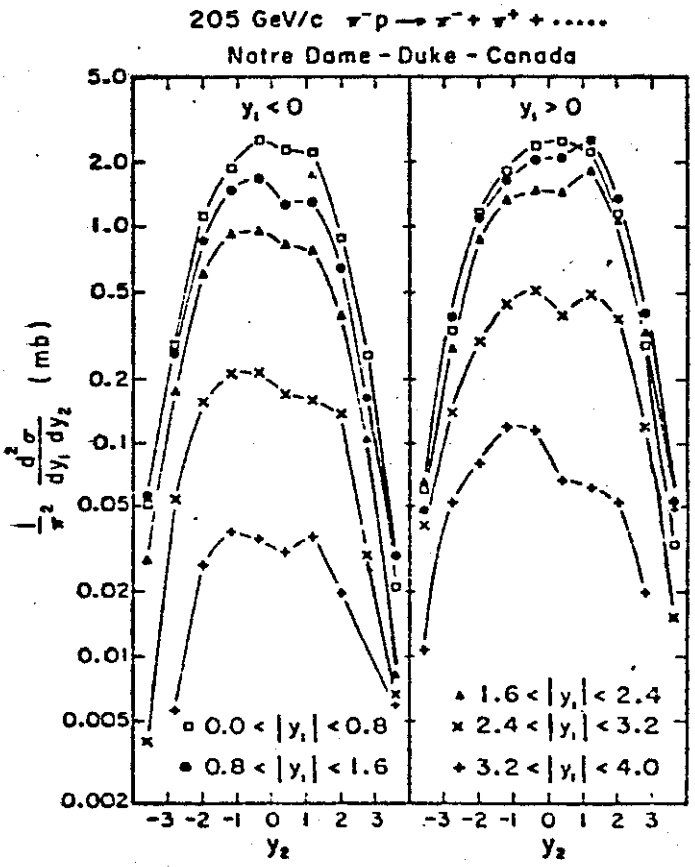

Fig. 9d

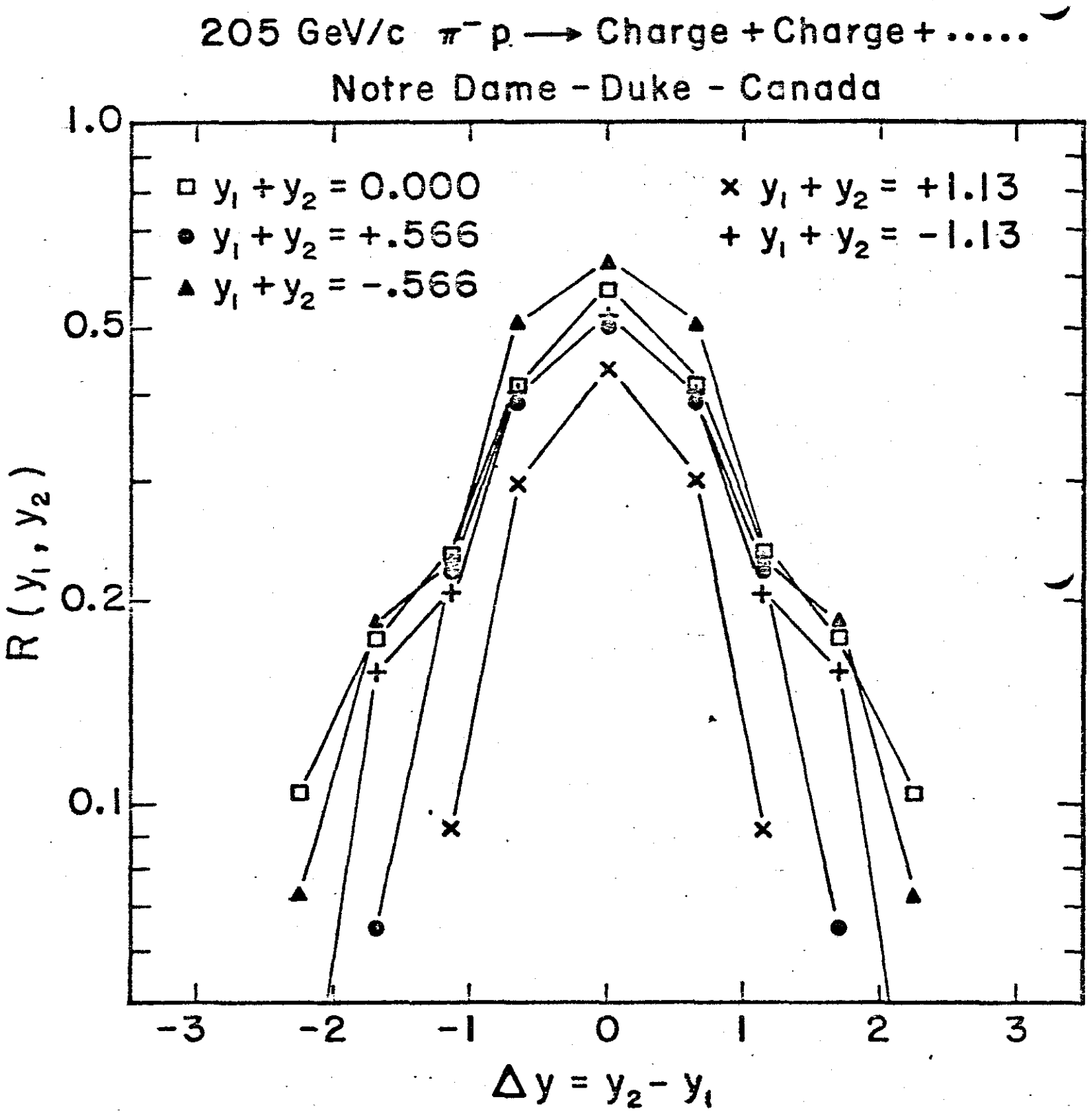
205 GeV/c $\pi^- p \longrightarrow$ Charge + Charge + ...
Notre Dame - Duke - Canada
$y_1 + y_2 = 0.000$
$y_1 + y_2 = +.566$
$y_1 + y_2 = -.566$
$y_1 + y_2 = +1.13$
$y_1 + y_2 = -1.13$
1.0
0.5
0.2
0.1
$R(y_1, y_2)$
-3
-2
-1
0
1
2
3
$\Delta y = y_2 - y_1$

Fig. 10